Supporting Information

Amplification of Polarization Ratio is Observed in Monolayer Dion-Jacobson Hybrid Perovskites

Dongying Fu,*[a,b] Yanli Ma,[a] Chang-Yuan Su,[c,d] Zhuo Chen,[a] and Da-Wei Fu*[c]

[a] Institute of Crystalline Materials, Shanxi University, Taiyuan, Shanxi 030006, P. R. China

[b] State Key Laboratory of Quantum Optics and Quantum Optics Devices, Shanxi University, Taiyuan, Shanxi 030006, P. R. China

[c] Institute for Science and Applications of Molecular Ferroelectrics, Key Laboratory of th e Ministry of Education for Advanced Catalysis Materials, Zhejiang Normal University, Jinhua, 321004, P.R. China
[d] Ordered Matter Science Research Center, Jiangsu Key Laboratory for Science and Applications of Molecular Ferroelectrics, Southeast University, Nanjing 211189, P.R. China

Table of Contents

Powder X-ray diffraction and single crystal structure determination.....2

Thermogravimetric (TGA) and Differential scanning calorimetry 2

UV-vis-NIR absorption spectroscopy and Second-Harmonic Generation and measurements.....2

The temperature-dependent dielectric measurements.....3

Photodetector device Preparation.....3

Computational Details.....3

Figure S1. Experimental and simulated PXRD patterns.....4

Figure S2. Thermogravimetric analysis curves.....4

Figure S3. The Pb-Br bond lengths in **2** and **1** at room temperature.....4

Figure S4. Average equatorial and axial Pb−Br−Pb angles in the structure.....5

Figure S5. The SHG intensity of **1** vs. particle size curves at 1064 nm.....5

Figure S6. Band structure and PDOS for **2** and **1**.....5

Figure S7 Photoresponse at different light power intensities under 377 nm.....6

Figure S8. Repeatability test of short circuit current for **1** at 377 nm and 405 nm.....6

Table S1 Crystal data and structure refinements for **1**.....7

Powder X-ray diffraction and single crystal structure determination:

Powder X-ray diffraction were performed on a Rigaku Ultimate IV diffractometer, and the diffraction patterns were collected from 5° to 40° with a step size of 0.02°. Single crystal structural data was performed on a Rigaku Saturn 724^+ diffractometer using Mo-Kα radiation (λ = 0.71073 Å) at different temperature. Crystal structures of **1** and **2** were solved by direct methods and then refined by the full-matrix method based on F^2 using the SHELXLTL software package. The data collection and structure refinement of **1** at room/high temperature phase was summarized in Table S1. The X-ray crystallographic structures have been deposited at the Cambridge Crystallographic Data Centre (deposition numbers CCDC: 2220208 (**1** at 301 K) and 2282804 (**1** at 420 K) and can be obtained free of charge from the CCDC via www.ccdc.cam.ac.uk/getstructures.

Thermogravimetric (TGA) and Differential scanning calorimetry (DSC) measurements:

TGA analysis was performed on a Setaram labsys evo Analyzer under nitrogen flow (30 mL/min) at a typical heating rate of 5 °C/min. DSC test was performed by heating and cooling the polycrystalline samples on a Perkin−Elmer Diamond DSC instrument in the temperature range300−400 K with a heating rate of 10 K/min under nitrogen atmospheric pressure in aluminum crucibles.

UV-vis-NIR absorption spectroscopy and Second-Harmonic Generation and measurements:

The UV-Vis absorption data were recorded at room temperature using a powdered $BaSO_4$ sample as a standard on a PERSEE-TU-1950 Uv-vis spectrophotometer. The scanning wavelength range is from 200 nm to 800 nm. Polycrystalline samples were ground to different particle sizes for the powder SHG measurements, using KH_2PO_4 (KDP) as a reference material. An unexpanded laser beam with low divergence (pulsed Nd:YAG at a wavelength of 1064 nm, 5 ns pulse duration, 1.6 MW peak power, 10 Hz repetition rate) was used. The instrument model was FLS 920 from Edinburgh Instruments, and the temperature was 300-420 with the cooling and heating rate of 10

K/min with the DE 202 system, while the laser was Vibrant 355 II instrument from OPOTEK.

The temperature-dependent dielectric measurements:

The polycrystalline samples were ground and press into flake. Silver conduction paste deposited on the flake surfaces was used as the electrodes. Complex dielectric permittivity was measured with a TH2828A impedance analyzer over the frequency range from 1 kHz to 1 MHz with an applied electric field of 0.5 V.

Photodetector device Preparation:

The planar structure photodetectors were assembled using the single-crystal devices of **1** and **2**. Before the device fabrication, the crystal was cleaned under nitrogen flow. Two symmetric Ag electrodes were coated on the flat side of **1** and **2** single crystal. Subsequently, the above obtained electrode was placed on the glass substrate for the measurement. Photodetection measurements were performed on a Keithley 6517 B electrometer under 377 and 405 nm lasers.

Computational Details:

First-principles based density functional theory (DFT) calculations have been conducted to explore the electronic properties of these compounds, which using the single crystal data of **1** and **2** at room temperature. The exchange and correlation effects were treated by Perdew-Burke-Emzerhoff in the generalized gradient approximation for solids. The core-electrons interactions were depicted by the norm-conserving pseudo potential.

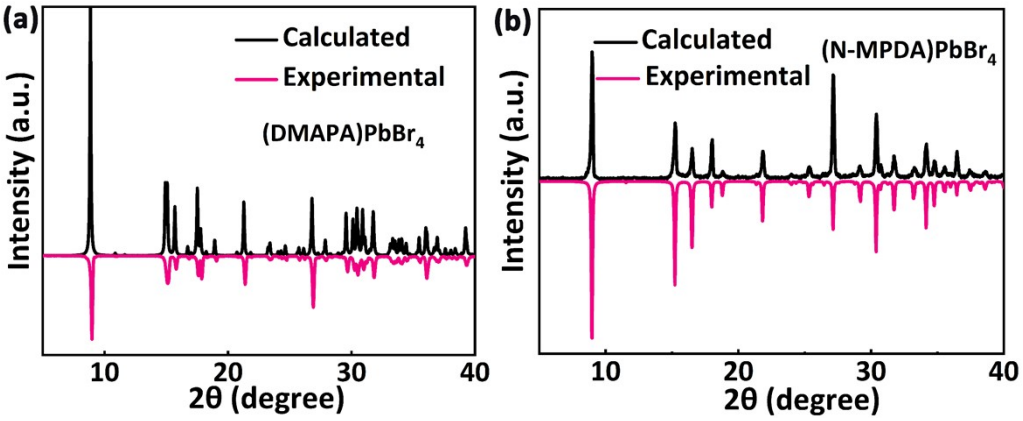

Fig. S1. Experimental and simulated PXRD patterns of **2** (a) and **1** (b).

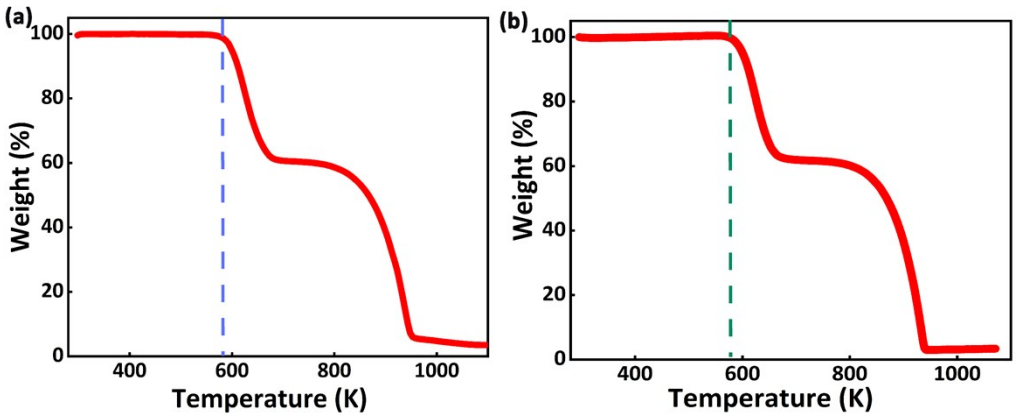

Fig. S2. Thermogravimetric analysis curves of **2** (a) and **1** (b).

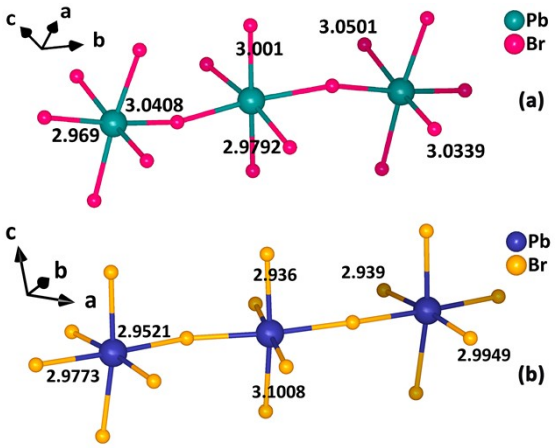

Fig. S3. The Pb-Br bond lengths in **2** (a) and **1** (b) at room temperature.

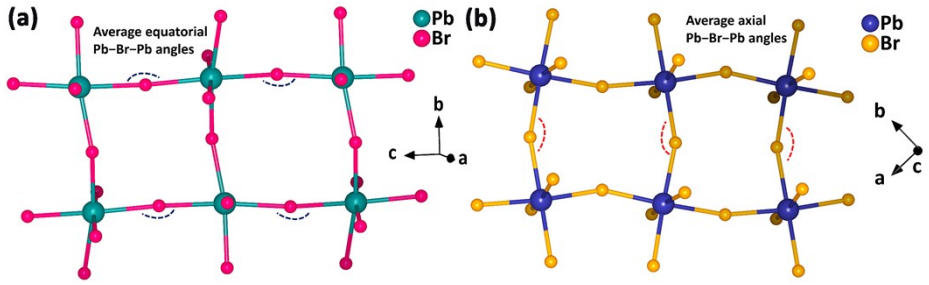

Fig. S4. Average equatorial and axial Pb−Br−Pb angles in the structure of **2** (a) and **1** (b).

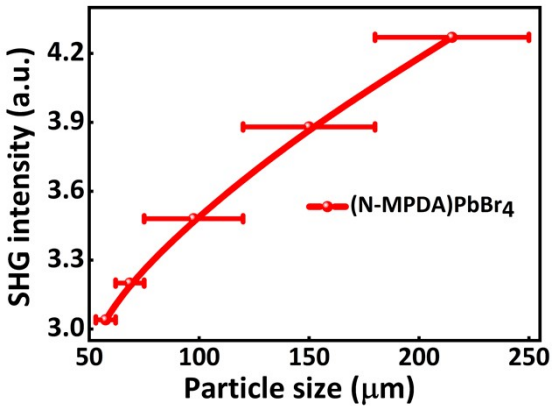

Fig. S5. The SHG intensity of **1** vs. particle size curves at 1064 nm. The solid curve is shown to guide the eyes, which is not fits to the data.

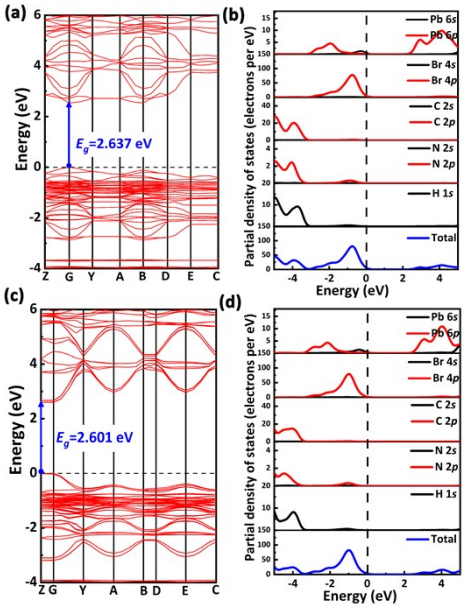

Fig. S6. Band structure (a) and PDOS (b) of **2**. Band structure (c) and PDOS (d) of **1**.

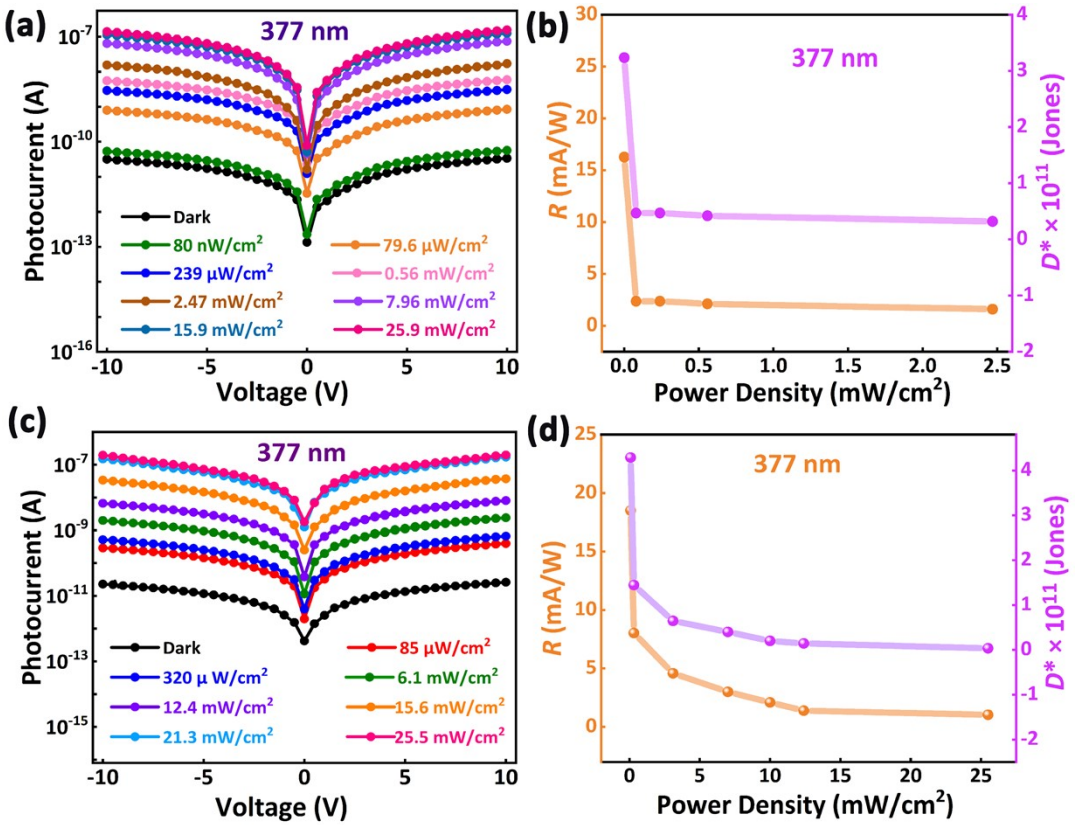

Fig. S7. Photoresponses under different light power intensities of the device based **2** (a) and **1** (c) under 377 nm. *R* and *D** values of **2** (b) and 1 (d) under 377 nm as a function of incident light power.

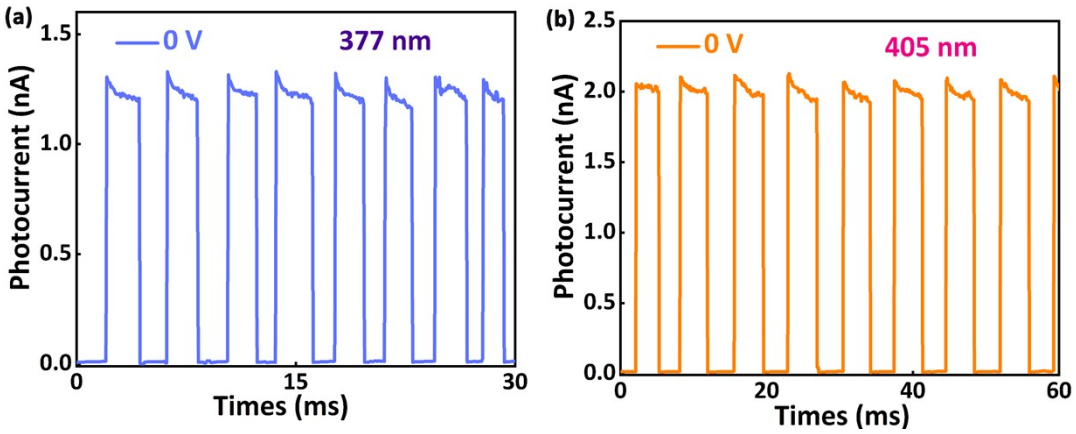

Fig. S8. Repeatability test of short circuit current for **1** at 377 nm (a) and 405 nm (b).

Table S1. Crystal data and structure refinements for **1** at room temperature and 420 K.

Compound	**1**	**1**
Temperature	301 K	420 K
Formula	$C_4H_{14}N_2PbBr_4$	$C_4H_{14}N_2PbBr_4$
Weight	617	617
Crystal system	Monoclinic	Monoclinic
Space group	*Pn*	*C*2/*c*
a (Å)	8.3185(8)	8.5255(8)
b (Å)	8.3196(6)	8.3313(6)
c (Å)	20.1444(16)	19.608(3)
α (°)	90	90
β (°)	101.654(4)	102.014(13)
γ (°)	90	90
V (Å^3)	1365.4(2)	1362.2(3)
Z	4	4
*ρ*calc g/cm^3	3.002	3.009
Rint	0.0683	0.0693
R_1	0.0471	0.0582
wR_2	0.1158	0.1408
GOF	1.098	1.074